Effect of doping on structural and superconducting properties in $Ca_{1-x}Na_xFe_2As_2$ single crystals ($x = 0.5, 0.6, 0.75$)

N. Haberkorn,[1] B. Maiorov,[1] M. Jaime,[2] I. Usov,[3] M. Miura,[1] G. F. Chen,[4] W. Yu,[4] and L. Civale[1]

[1]*MPA-STC, Los Alamos National Laboratory, Los Alamos, New Mexico 87545, USA*

[2]*MPA-CMMS, Los Alamos National Laboratory, Los Alamos, New Mexico 87545, USA*

[3]*MST-7, Los Alamos National Laboratory, Los Alamos, New Mexico 87545, USA*

[4]*Department of Physics, Renmin University of China, Beijing 100872, China*

(Received 21 April 2011; revised manuscript received 24 June 2011; published 30 August 2011)

We study the correlation between crystalline structure and superconducting properties in Na-doped $Ca_{1-x}Na_xFe_2As_2$ single crystals for three chemical compositions ($x = 0.5$, 0.6, 0.75). We find the maximum superconducting transition temperature $T_c \sim 33.4$ K at $x \sim 0.75$. The Na substitution causes the decrease of the *a-b* crystallographic axes and the increase of the *c* axis in the tetragonal phase. The single crystals show perfect diamagnetism, indicating full superconducting volume. The anisotropy ratio for the upper critical field near the superconducting transition temperature is $\gamma = 1.85 \pm 0.05$, independently of the Na content. A narrow vortex liquid phase was detected in the sample with highest T_c ($x = 0.75$), consistent with the expectations based on a Lindemann criterion. The analysis of the critical currents shows no evidence of correlated pinning and indicates that the pinning arises from a combination of several mechanisms. At low fields, pinning by random nanoparticles dominates. At higher fields, a small and field independent J_c in the optimally doped crystal may originate in the simultaneous presence of sparse large nanoparticles and a much denser distribution of smaller particles, with the sparse pins producing a caging effect that constrains the volume of the vortex bundle associated with the denser and weaker defects.

DOI: 10.1103/PhysRevB.84.064533 PACS number(s): 74.70.Xa, 74.25.Op, 74.25.Sv

I. INTRODUCTION

Since the discovery of superconductivity in iron pnictide superconductors with $T_c \sim 26$ K in LaFeAsO(F), much effort has been focused on finding new compounds.[1,2] These materials exhibit a variety of physical properties and ground states, e.g., spin density waves and superconductivity.[2] In the AFe_2As_2 family (122, A: Ca, Sr, Ba), the properties are strongly influenced by doping. The ternary iron arsenide $CaFe_2As_2$ is an antiferromagnet that exhibits no superconductivity, but superconductivity can be induced by partial chemical substitution of Ca by Na,[3–5] substitution of As by P,[6] or with applied pressure.[7,8] Recently, a $T_c \sim 33$ K was reported in $Ca_{1-x}Na_xFe_2As_2$ with $x \sim 0.66$.[9] This is the highest T_c observed for this compound and, interestingly, it is reached for a higher hole doping than in other 122 systems such as $(Ba,K)Fe_2As_2$ and $(Sr,K)Fe_2As_2$, where the best T_c (38 and 35 K, respectively) occurs for $x \sim 0.4$.[10,11] Clearly, the superconducting properties of the hole-doped 122 pnictides are not determined only by doping level because the interband coupling between the hole and electron bands also plays an important role. The observed differences in the superconducting properties of different 122 pnictides are attributed to different relative filling factors of the electron and hole Fermi pockets[12,13] that constitute their Fermi surfaces.

The layered structure in pnictides induces anisotropy in the electronic properties, but in contrast to the case of single-band materials, the angular dependence of the superconducting parameters can not be described by a single temperature-independent anisotropy parameter γ. Indeed, if we use the usual definition $\gamma = H_{c2}^{ab}/H_{c2}^{c}$, where H_{c2}^{ab} and H_{c2}^{c} are the upper critical fields along the *ab* plane and *c* axis, respectively, then γ is temperature (T) dependent. In addition, $H_{c2}(T,\Theta)$, where Θ is the angle between the applied magnetic field **H** and the crystallographic *c* axis, does not follow the standard dependence $H_{c2}(T,\Theta) = H_{c2}(T,\Theta = 0)/\varepsilon(\Theta)$, where $\varepsilon(\Theta) = (\cos^2\Theta + \gamma^{-2}\sin^2\Theta)^{1/2}$, and can even exhibit two maxima at $\mathbf{H}\|c$ and $\mathbf{H}\|ab$.[14] These unconventional features are commonly attributed to the multiband nature of superconductivity in these compounds.[15–17] Most studies in 122 iron arsenides show that $\gamma \sim 2$ close to T_c and decreases to values near 1 at low temperatures.[16] This $\gamma(T)$ dependence looks similar in all the 122 materials, independently of the carrier nature.[16,18,19] One exception was reported for pressure-induced superconductivity in $CaFe_2As_2$ single crystals, where γ is close to 1 near T_c (12 K) and increases to $\gamma \sim 1.2$ at $\sim T_c/2$.[7] Considering these results and the difference in the chemical doping dependence of T_c in $Ca_{1-x}Na_xFe_2As_2$, more studies are necessary to clarify the influence of the doping on T_c and anisotropic properties.

In a related topic, several studies in 122 pnictides discuss the existence of a liquid phase in the vortex phase diagram.[20–22] In cuprate superconductors, the presence of an extended vortex liquid phase is associated with the high T_c and concomitant small coherence length (ξ), and the high γ (~5–7 in $YBa_2Cu_3O_{7-\delta}$ and >100 in Bi-based compounds). In the pnictide superconductors, the large number of compounds with tunable doping levels gives rise to a broad range of T_c and anisotropies. This opens up the possibility of a rich variety of vortex phase diagrams, but on the other hand, the smaller T_c and γ as compared to high-T_c superconductivity (HTS) oxides may result in a narrower or even absent vortex liquid phase. A vortex melting transition has been observed in $Ba_{1-x}K_xFe_2As_2$ (Refs. 21 and 22) and in Co-doped $BaFe_2As_2$ films.[23] However, the mechanisms that govern the solid-liquid

transition in pnictide superconductors are still not fully understood. For example, the temperature-dependent anisotropy, the coexistence of superconductivity and antiferromagnetism,[24] and the presence of anomalous magnetization effects[25] may all have a significant role in the vortex dynamics of these materials.

In this paper, we study the effects of Na chemical doping on the crystalline structure and superconducting properties of $Ca_{1-x}Na_xFe_2As_2$ single crystals. We analyze the effect of the charge carrier density on the H_{c2} anisotropy in single crystals (SC) with very different T_c's, where a chemical doping of $x \sim 0.5$ and 0.75 induces T_c's of 19 and 33 K, respectively. Our results show that the anisotropy of all the samples can be modeled with a single-band anisotropy with $\gamma \sim 1.85$ for $T \sim T_c$ independently of the doping level. In the SC with $T_c \sim 33$ K, we detect the presence of a narrow vortex liquid phase in agreement with the Lindemann criterion for the superconducting parameters T_c, H_{c2}, and the Ginzburg number (G_i).[26]

II. EXPERIMENTAL PROCEDURES

The single crystals were grown by the self-flux technique. The starting composition ratio was selected as $Na_{1.0}Ca_{0.3}Fe_2As_2$. The mixtures of NaAs, CaAs, FeAs, and Fe_2As were put into an alumina crucible and sealed in a Ta crucible under 1.6 atmosphere of argon gas. The Ta crucible was then sealed in an evacuated quartz ampoule and heated to 1160 °C and cooled slowly at 5 °C/h to grow single crystals. $Ca_{1-x}Na_xFe_2As_2$ single crystals with three different chemical compositions were selected for this study: $x = 0.50 \pm 0.05$ ($x = 0.5$); $x = 0.60 \pm 0.05$ ($x = 0.6$), and $x = 0.75 \pm 0.05$ ($x = 0.75$). The phase purity for each crystal was checked by x-ray diffraction (XRD) using a four-circle diffractometer goniometer. The composition was determined by energy dispersive x-ray (EDX) analysis and Rutherford backscattering.

The T and **H** dependence of the magnetization was studied using a superconductor quantum interference device (SQUID) magnetometer. Electrical resistivity was measured using the four-probe technique. The samples were mounted in a rotatable probe and the measurements were performed in applied magnetic fields between 0 and 15 T. Resistivity data were taken with an ac resistance bridge using a current density of $\sim$30 A cm^{-2}. Transport measurements were conducted with applied current (**J**) perpendicular to **H** in a maximum Lorentz force configuration.

All the single crystals exhibit a plateletlike morphology with the c axis perpendicular to the plane of the plate. At least two samples of each composition were initially characterized by magnetization and consistent results were obtained. In all cases, a 100% superconducting volume fraction was observed (see lower critical fields section). For the detailed studies on the crystals with $x = 0.5$ and 0.75, we used the same pieces for magnetization and transport, which in both cases can be approximated by parallelepipeds with dimensions (l, w, t) of $1.0 \times 0.145 \times 0.028$ mm^3 and $0.8 \times 0.655 \times 0.042$ mm^3, respectively.

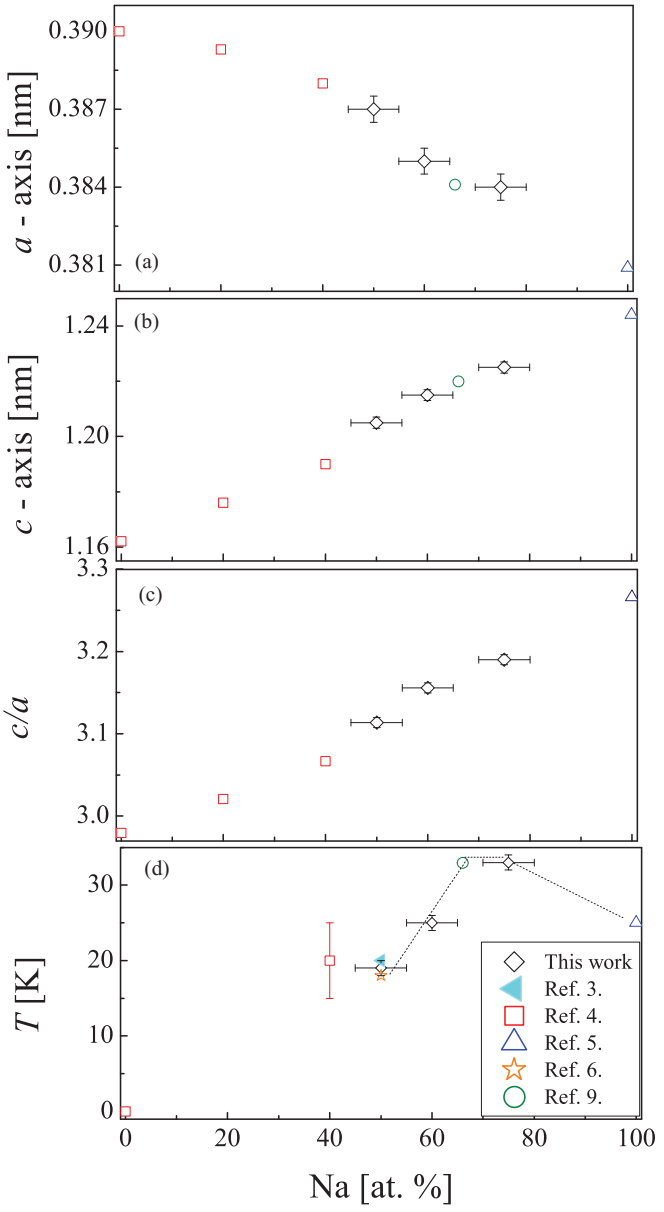

FIG. 1. (Color online) Na doping dependence in $Ca_{1-x}Na_xFe_2As_2$ of (a) lattice parameter a; (b) lattice parameter c; (c) c/a ratio; and (d) superconducting critical temperature T_c.

III. RESULTS

A. Crystalline structure

The chemical composition for each SC was determined by averaging of 20 measurements at different locations on the sample. The peaks were indexed on the basis of a tetragonal $ThCr_2Si_2$-type structure as was previously reported.[3,10] Figures 1(a) and 1(b) show the lattice parameters derived from the (00l), (012), (013), and (112) reflections. These results are in agreement with previously reported data, which are also included for comparison.[3–6,9] We observe that an increase in the sodium doping leads to an increase of the c axis and a compression in the a-axis parameter, resulting in an increase of the c/a ratio as shown in Fig. 1(c).

B. Superconducting transition temperature

The T_c of the three crystals was determined by magnetization measurements at low magnetic fields (~1.5 Oe) parallel to the c axis after performing a zero-field cooling; the composition dependence is shown in Fig. 1(d). Electrical transport measurements were performed on $x = 0.5$ and 0.75, which show the minimum and maximum T_c, respectively. Figure 2 shows normalized resistance $[R/R(T_c,H=0)]$ versus T at several H applied along the c axis. The data are normalized to the normal state resistivity (ρ_N), defined as ρ at the onset of the superconducting transition for $\mathbf{H} = 0$. The T_c values for $x = 0.5$ and 0.75, obtained from the $H = 0$ curves and defined as the intersection of linear fits to $\rho(T)$ in the normal state and transition regions (see sketch in Fig. 2) are ~19.4 and ~33.4 K, respectively, consistent with Fig. 1(d). These T_c values are in agreement with those previously reported, also included in Fig. 1(d), and clearly demonstrate that the highest T_c in this compound occurs at a doping different than in other 122 materials.[10,11] The transition in $x = 0.75$ shows a small but clear structure that may be associated with chemical inhomogeneity, however, it is rather sharp, with a total $\Delta T_c \sim 0.5$ K. Furthermore, if we consider the portions of $\rho(T)$ above and below the structure as the transitions of two samples, each individual transition is extremely sharp, with $\Delta T_c \sim 0.1$ K. Considering that thermal fluctuations impose a minimum transition width $\Delta T_c \geqslant G_i^* T_c$, this sets an upper limit $G_i \leqslant 3 \times 10^{-3}$ for $x = 0.75$. The transition in $x = 0.5$ is significantly wider, i.e., $\Delta T_c \sim 2$ K.

C. Upper critical fields

We now turn to the $R(T)$ in applied magnetic fields in Fig. 2. We note that both samples show appreciable magnetoresistance in the normal state, the effect being stronger in $x = 0.5$ than in $x = 0.75$. While this feature warrants further investigation, it is beyond the scope of this paper. The upper critical fields (H_{c2}) are determined using the same criterion

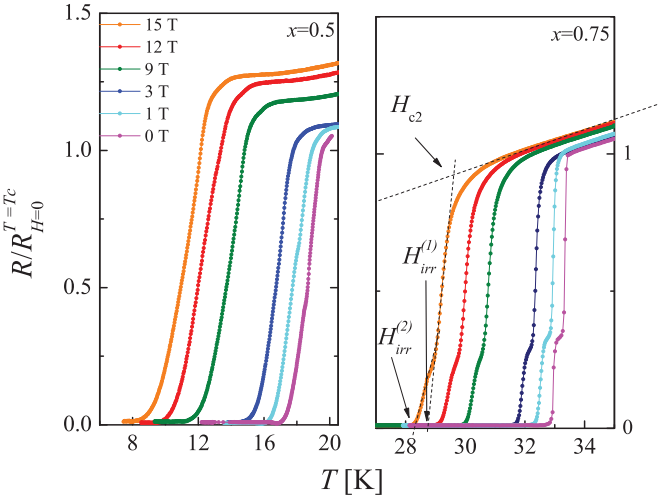

FIG. 2. (Color online) Resistance/resistance (T_c, $H = 0$) versus temperature (T) measurements at different applied magnetic field (H) along the c axis in the two studied single crystals. $x = 0.5$ (left panel); $x = 0.75$ (right panel).

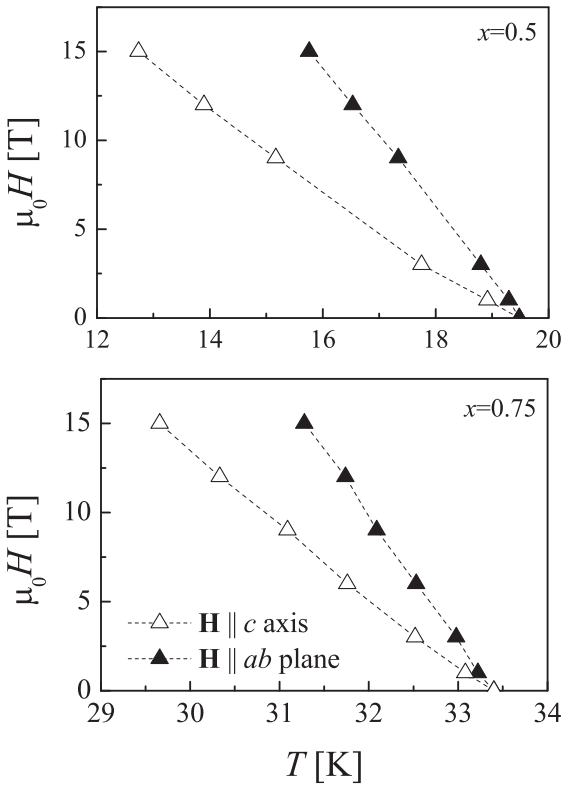

FIG. 3. Temperature dependence of the upper critical fields (H_{c2}) in $Ca_{1-x}Na_xFe_2As_2$ single crystals. $x = 0.5$ (upper panel); $x = 0.75$ (lower panel).

previously described for T_c. Also indicated in Fig. 2 is the criterion for the determination of the irreversibility field (H_{irr}), to be discussed below.

Figures 3(a) and 3(b) show H_{c2} versus T with $\mathbf{H}\|c$ and $\mathbf{H}\|ab$ for $x = 0.5$ and 0.75, respectively. To a good approximation, $H_{c2}(T)$ is linear in all cases, with average slopes

$$-\left.\frac{\partial H_{c2}^{ab}}{\partial T}\right|_{T_c} = 4\,\mathrm{T/K}, \quad -\left.\frac{\partial H_{c2}^{c}}{\partial T}\right|_{T_c} = 2.2\,\mathrm{T/K} \quad \text{for } x = 0.5$$

and

$$-\left.\frac{\partial H_{c2}^{ab}}{\partial T}\right|_{T_c} = 7.15\,\mathrm{T/K}, \quad -\left.\frac{\partial H_{c2}^{c}}{\partial T}\right|_{T_c} = 4\,\mathrm{T/K} \quad \text{for } x = 0.75.$$

Using the standard definition of anisotropy, for each sample, the ratio of the $H_{c2}(T)$ linear slopes for $\mathbf{H}\|c$ and $\mathbf{H}\|ab$ gives γ, which in both cases is temperature independent in the measured range within our experimental error. Remarkably, we obtain the same value for both crystals, $\gamma = 1.85 \pm 0.05$.

Considering that multiband effects are known to produce anomalous $H_{c2}(\Theta)$ dependences, measurements for $\mathbf{H}\|c$ and $\mathbf{H}\|ab$ are not enough to fully determine the angle-dependent behavior in these superconductors.[14,16] To further explore this issue, we measured $\rho(T)$ at constant H at different orientations to extract $H_{c2}(T,\Theta)$ values [and also $H_{irr}(T,\Theta)$, to be discussed below]. As examples, the $T_{c2}(\Theta)$ data obtained from $\rho(T)$ at $\mu_0 H = 12$ T for both crystals are shown in Fig. 4. The dotted lines represent the anisotropic scaling using the $H_{c2}(T,\Theta = 0)$ data from Fig. 3 and $\gamma = 1.85$. In a single-band anisotropic superconductor, if the appropriate γ

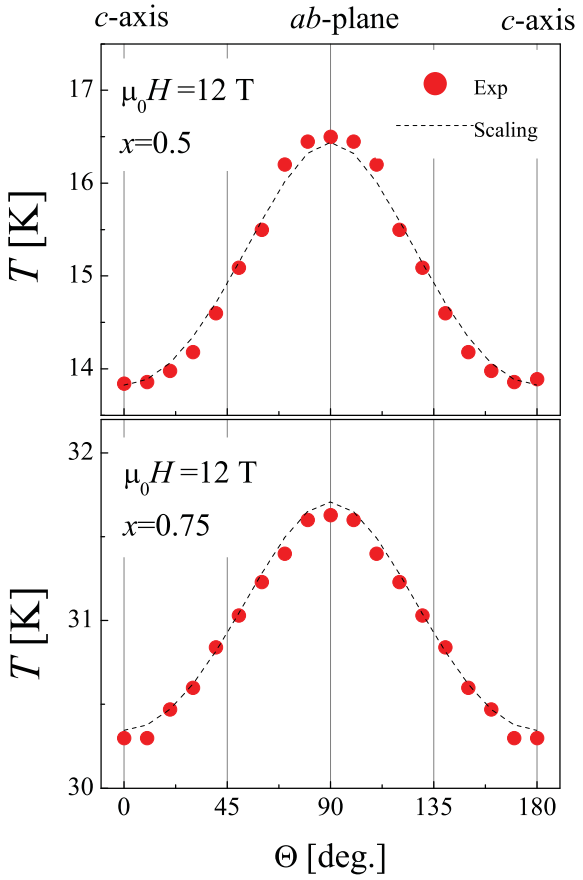

FIG. 4. (Color online) $T_{c2}(H)$ vs angle (Θ) at 12 T. $x = 0.5$ (upper panel); $x = 0.75$ (lower panel).

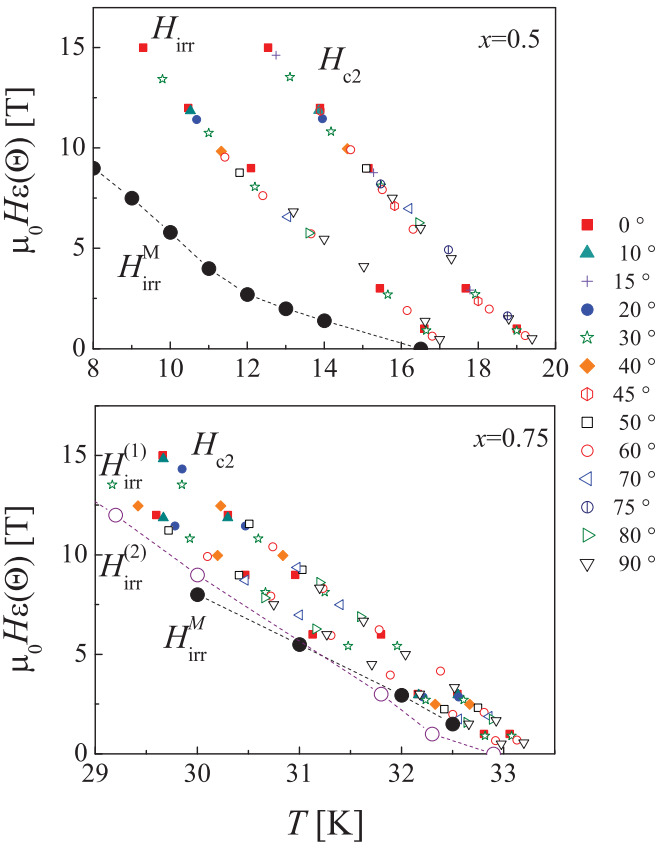

FIG. 5. (Color online) Anisotropic scaling of H_{c2} and H_{irr} from electrical resistivity, and H_{irr} from magnetization data with $\mathbf{H}\|c$ axis (H_{irr}^{M}). $x = 0.5$ (upper panel); $x = 0.75$ (lower panel). For $x = 0.75$, the H_{irr} values obtained from the two definitions sketched in Fig. 2 are included.

is used, all the $H_{c2}(T,\Theta)$ data should collapse on a single curve $\tilde{H}_{c2}(T) = H_{c2}(T,\Theta)\varepsilon(\Theta)$. Figures 5(a) and 5(b) show $\tilde{H}_{c2}(T)$ for $x = 0.5$ and 0.75, respectively. Both curves in Fig. 5 include data measured at $\mu_0\mathbf{H} = 0$, 1, 3, 6, 9, 12, and 15 T, and several orientations (including 0 and 90°) as indicated by the various symbols. In both samples, the curves collapse on a single curve using a $\gamma \sim 1.85 \pm 0.05$, indicating that all our $H_{c2}(T,\Theta)$ data in both crystals are well described by a single-band anisotropic model. It is important to mention, however, that H_{c2} for multiband superconductors behaves as in a single-band material close to T_c.[14] Our field range allows us to access the full angular range for reduced temperatures $t = T/T_c > 0.81$ for $x = 0.5$ and 0.94 for $x = 0.75$. As mentioned in the Introduction, in most 122 pnictides, $\gamma \sim 2$ close to T_c and decreases to ~ 1 at low temperatures.[16,22] High-field studies would be required to investigate the low-temperature anisotropy in our crystals.

Assuming the validity of the single-band description in our temperature range, we can calculate the superconducting coherence length (ξ) by combining (Ref. 27)

$$H_{c2}(T) = \frac{\Phi_0}{2\pi\xi^2(T)} \quad \text{with} \quad \xi(T) = 0.74\frac{\xi_0}{\sqrt{1-t}}.$$

Thus,

$$\xi_0^2 = \frac{\Phi_0}{1.1\pi T_c}\left[\frac{\partial H_{c2}^c}{\partial T}\bigg|_{T_c}\right]^{-1}.$$

We obtain $\xi_0^c = 3.68$ nm and $\xi_0^{ab} = 1.94$ nm for $x = 0.5$, and $\xi_0^c = 2.08$ nm and $\xi_0^{ab} = 1.09$ nm for $x = 0.75$. Although these numbers do not necessarily represent the real ξ_0 values at low temperatures, where the multiband effects may become relevant, they do reflect the energy scale associated with the effective superconducting gap in the explored region. From very basic considerations $\xi_0 \propto v_F/T_c$, where v_F is the Fermi velocity. The product $\xi_0 T_c$ is 71.4 nm K and 69.5 nm K for $x = 0.5$ and 0.75, respectively, indicating that v_F is the same in both crystals within our resolution. In particular, for a weakly coupled BCS superconductor $\xi_0 = 0.18\frac{\hbar v_F}{k_B T_c}$, so in that limit we would obtain $v_F \sim 5 \times 10^6$ cm/s in both cases.[27]

D. Lower critical fields

We determined the lower critical fields (H_{c1}) using SQUID magnetometry. After zero-field cooling of the crystal from above T_c to the desired temperature, we measured the initial magnetization $M(H)$. For each T, we identified the field H_{dev}, where $M(H)$ deviates from the initial linear dependence $M = -\frac{V}{4\pi(1-\eta)}H$ corresponding to the Meissner state response (perfect diamagnetism), where V is the crystal volume and η is the appropriate demagnetizing factor. For both single crystals, we performed these measurements for both $\mathbf{H}\|c$ and $\mathbf{H}\|ab$, in

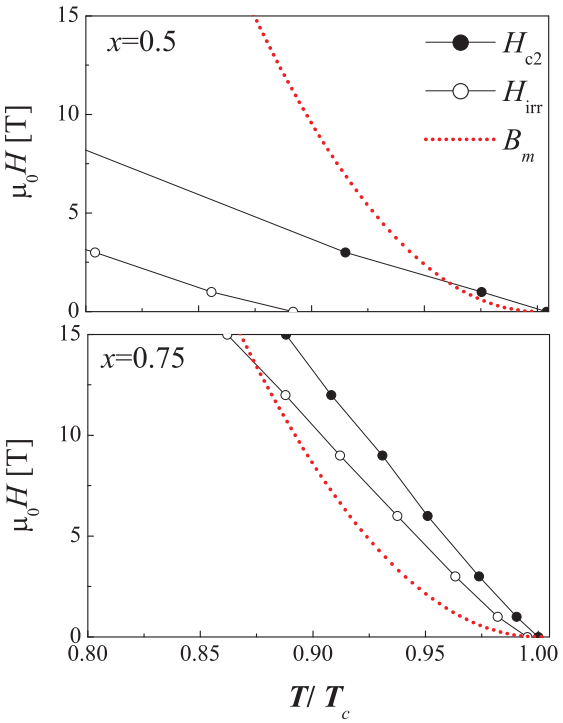

FIG. 6. (Color online) Temperature dependence of the vortex melting field (B_m) estimated from the Lindemann criterion, and the upper critical fields (H_{c2}) and irreversibility fields (H_{irr}) from electrical resistivity with $\mathbf{H}\|c$ axis in $Ca_{1-x}Na_xFe_2As_2$ single crystals. $x=0.5$ (upper panel); $x=0.75$ (lower panel).

the last case with **H** parallel to the longest crystal dimension l.[26] Using the simple estimates $\eta_c \sim 1 - t/l - t/w$ and $\eta_{ab} \sim t/l$ for $\mathbf{H}\|c$ and $\mathbf{H}\|ab$, respectively, we obtain $\eta_c \sim 0.78$ and $\eta_{ab} \sim 0.028$ for $x=0.5$, and $\eta_c \sim 0.88$ and $\eta_{ab} \sim 0.053$ for $x=0.75$. For both crystals, we used the measured slopes of the linear M versus H Meissner responses in both orientations to confirm that the superconducting volumes coincide with the physical volumes (l, w, t) and that the η factors agree with the calculations within our resolution.

For $\mathbf{H}\|ab$, we roughly estimated

$$H_{c1}^{ab}(T) = H_{dev}(T)/(1-\eta_{ab}) \approx H_{dev}(T).$$

From (Ref. 27)

$$H_{c1}^{ab} \approx \frac{\Phi_0}{4\pi\lambda_{ab}\lambda_c}(\ln\kappa + 0.5),$$

where λ_{ab} (λ_c) are the London penetration depths for $\mathbf{H}\|c$ ($\mathbf{H}\|ab$) and $\kappa = (\lambda_{ab}\lambda_c/\xi_{ab}\xi_c)^{1/2}$ is the Ginzburg-Landau parameter, at $T=5$ K we obtain $(\lambda_{ab}\lambda_c)^{1/2} = 198$ nm and $\kappa = 82$ for $x=0.5$, and $(\lambda_{ab}\lambda_c)^{1/2} = 136$ nm and $\kappa = 91$ for $x=0.75$. In principle, we could use the measurements for $\mathbf{H}\|c$ to determine H_{c1}^c and thus λ_{ab}; however, we found that for that orientation, vortex pinning produces a large irreversible magnetization signal (due to the larger demagnetizing effects) that makes the determination of H_{dev} unreliable.

E. Irreversibility lines

To determine the irreversibility field $H_{irr}(T,\Theta)$, from transport data as that shown in Fig. 2, we identified the point where $R/R(T_c,H=0)$ becomes zero for each magnetic field. In $x=0.75$, we need to take into account the presence of the structure that is visible at all fields. Thus, for each field and orientation, we defined two extrapolations to $\rho=0$, one from each portion of the transition, as sketched in Fig. 2. Figures 5(a) and 5(b) show $\tilde{H}_{irr}(T) = H_{irr}(T,\Theta)\varepsilon(\Theta)$for $x=0.5$ and 0.75, respectively. The first observation is that for both crystals all the data collapse on a single curve, as in the case of H_{c2}(T,Θ), for the same $\gamma = 1.85 \pm 0.05$, consistent with a single-band anisotropic description, and indicating that H_{irr} is governed random pointlike defects.[28]

The next question is whether H_{irr} represents a real phase transition, and thus the region between $\tilde{H}_{irr}(T)$ and $\tilde{H}_{c2}(T)$ is a vortex liquid phase. In the case of $x=0.75$, it is apparent from Fig. 5(b) that the $\tilde{H}_{irr}(T)$ and $\tilde{H}_{c2}(T)$ curves spread apart monotonically as H increases [for both criteria used to define $\tilde{H}_{irr}(T)$]. Moreover, $\tilde{H}_{irr}(T)$ exhibits small upward concavity that is absent $\tilde{H}_{c2}(T)$; fits to $H \propto (1-T/T_c)^n$ give $n=1$ for H_{c2} (as expected for a single-band description) and $n=1.1$ for H_{irr}. This suggests that $\tilde{H}_{irr}(T)$ in $x=0.75$ represents a true solid-liquid phase transition, and in that case the good anisotropic scaling indicates that it is associated with random disorder, similar to the case of a vortex-glass transition. In contrast, if correlated pinning were dominant, a peak in $H_{irr}(\Theta)$ would appear when **H** is parallel to the defects, as frequently observed in YBCO and as we have recently found in Co-doped 122 films.[14] In the case of $x=0.5$, the situation is less clear, as the broader transition at $H=0$ precludes us from reaching a definitive conclusion about the presence of a liquid phase.

It is instructive to compare these results with a simple estimate of the vortex-lattice melting line (B_m) based on the Lindemann criterion

$$B_m(T) \approx \left(5.6c_L^4/G_i\right)H_{c2}(1-T/T_c)^2,$$

where $c_L \approx 0.1$–0.4 and the Ginzburg number $G_i = \frac{1}{2}[\frac{\gamma T_c}{H_c^2(0)\xi^3(0)}]^2$.[26] Using the experimental values for ξ_{ab}, and assuming that in both crystals $\lambda_c = \gamma\lambda_{ab}$ with $\gamma = 1.85$ (thus $\lambda_{ab} = 146$ nm for $x=0.5$ and 100 nm for $x=0.75$), we can estimate $G_i \sim 1.5 \times 10^{-5}$ and $\sim 3 \times 10^{-5}$ for $x=0.5$ and 0.75, respectively. There is, of course, a very large uncertainty in $B_m(T)$ due to the c_L^4 factor, but we can consider $c_L = 0.1$ and estimate the locus of the lowest possible $B_m(T)$ line. The comparison between our $H_{irr}(T)$ and $H_{c2}(T)$ data and such a line is shown in Figs. 6 and 6(b), and it indicates that, according to this simple analysis, a vortex liquid phase is possible in the $x=0.75$ with $T_c \sim 33.4$ K, whereas this is unlikely in the $x=0.5$ with $T_c \sim 19.4$ K.

F. Magnetization measurements of pinning properties

We determined the magnetic field dependence of the critical-current density [$J_c(H)$] for $x=0.5$ and 0.75 by applying the critical-state Bean model to the magnetization data obtained in hysteresis loops. For $\mathbf{H}\|c$ (i.e., **H** parallel to t, the shortest sample dimension), $J_c = \frac{20\Delta m}{tw^2(l-w/3)}$, where Δm is the difference in magnetic moment between the top and

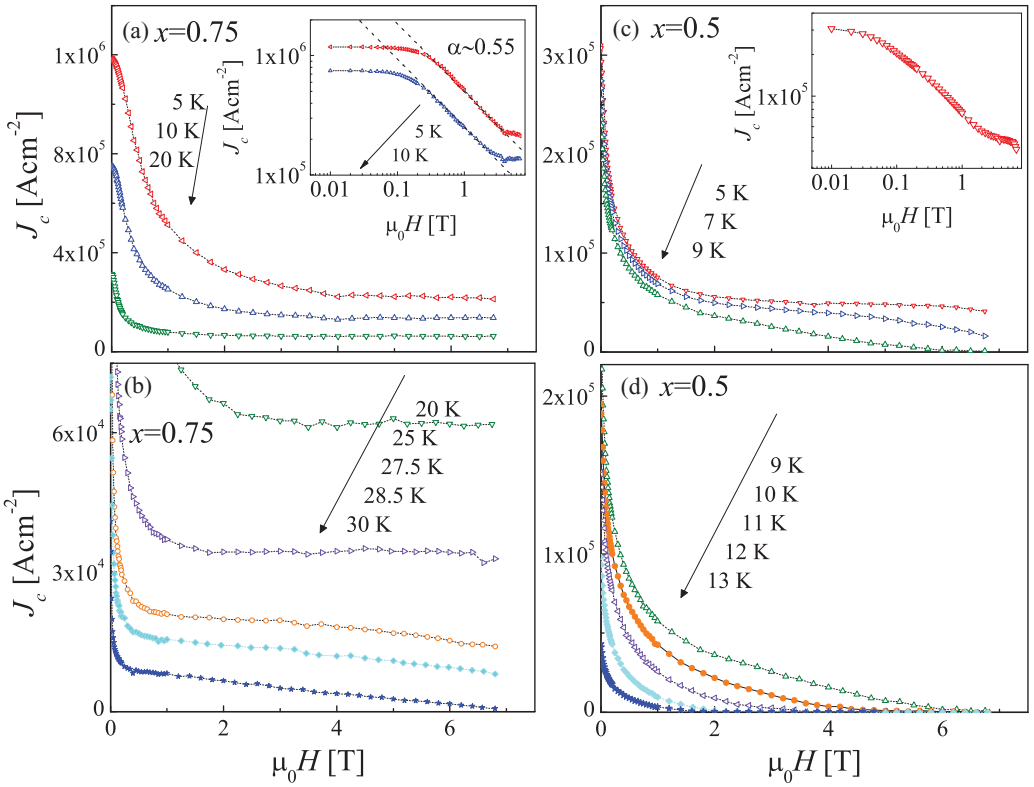

FIG. 7. (Color online) (a) Critical-current density (J_c) as a function of magnetic field (H) in $Ca_{1-x}Na_xFe_2As_2$ single crystals. (a) and (b) $x = 0.75$. (c) and (d) $x = 0.5$. Insets in (a) and (c) show log-log plots.

bottom branches of the hysteresis loop, and t, w, and l are the thickness, width, and length of the sample ($l > w$), respectively. Figure 7 shows a summary of the results for this orientation.

We first discuss the $x = 0.75$ results [Figs. 7(a) and 7(b)]. At low fields, J_c is independent of H, as seen in the log-log scale in the inset of Fig. 7(a). We will identify this as regime I (the regimes are indicated in Fig. 8, discussed below). As H increases, we observe that J_c follows a power law $J_c \propto H^{-\alpha}$ with a $\alpha \sim 0.55$ (regime II) [see inset of Fig. 7(a)]. A regime III shows a field range where $J_c(H) \sim constant$, which over a wide range of temperatures ($T < 25$ K) extends up to our maximum magnetic field $H \sim 6.5$ T. Finally, above 25 K, we observe that J_c decreases when H increases (regime IV), and goes to zero at H_{irr}. Crystal $x = 0.5$ shows some qualitative similarities. An initial $J_c(H) \sim constant$ (regime I) is also present, but constrained to even lower H than in $x = 0.75$, followed by a field range where J_c decreases with H (regime II), but no clear power-law dependence is observed. For higher H, another $J_c(H) \sim constant$ region occurs (regime III), but only at low T and over a more restricted H range, and finally J_c decreases with H (regime IV) until $J_c(H) = 0$ at H_{irr}.

Next, we investigated whether any of these regimes were associated with correlated pinning arising from parallel columnarlike defects, which can occur naturally as in the case of dislocations[29] and domain walls.[30] Although the angular dependence of H_{irr} rules out measurable correlated pinning in that region of the H-T plane, it could still occur significantly deeper in the solid phase. To explore this possibility, we measured hysteresis loops with the c axis of the crystal tilted by 30° from **H**. In this configuration, the current flowing along one pair of sides of the rectangular crystal is no longer in maximum Lorentz force configuration, so the effective J_c in those sides (that we chose to be the short ones, w) is $J_c/\cos(30°)$, and using the anisotropic version of the critical-state Bean model, we obtain $J_c = \frac{20\Delta m}{tw^2(l-\frac{w}{3\cos(30°)})}$. Figure 8 shows the comparison between J_c for $\mathbf{H}\|c$ axis and **H** rotated 30° from the c axis as a function of $\varepsilon(\Theta)H$, the effective field in the anisotropic scaling scheme, with $\gamma = 1.85$ as obtained from transport measurements. We observe an almost perfect coincidence between data at both orientations for all temperatures and fields, indicating that $J_c(H,\Theta) = J_c[\varepsilon(\Theta)H]$ as expected in a scenario based on random disorder and the anisotropic scaling approach, and ruling out the presence of correlated pinning.

IV. DISCUSSION

A. Analysis of the pinning mechanisms

Some previous studies of $J_c(H)$ in hole- and electron-doped 122 single crystals showed the presence of a second peak in the magnetization (SPM), known as fishtail effect,[31] which occurs for $\mathbf{H}\|c$ but is absent for $\mathbf{H}\perp c$.[32] This SPM was attributed to small-size normal-core pinning. Also, vortex creep analysis suggests that it results from a crossover from elastic to plastic creep.[32] We do not observe a SPM in our crystals at any temperature or field orientation, pointing to different pinning mechanisms and/or regimes. It is, thus,

important to compare and contrast our samples with those of previous reports and to explore their pinning properties in detail.

It is clear that the whole $J_c(H)$ curves shown in Figs. 7 and 8 can not be explained using a single type of pinning centers. Similarly to what is observed in many superconductors, regime I can be associated with single-vortex pinning, crossing over to regime II ($J_c \propto H^{-\alpha}$) when the vortex density increases to the point that their interactions become important. But then, the next $J_c(H) \sim constant$ (regime III) can not arise from single-vortex pinning by the same defects, thus more than one source of pinning must be at play in these crystals. The simplest possibility is that regimes I and II are due to a sparse distribution of strong random defects, and regime III to a denser collection of smaller and weaker defects.

B. Regimes I and II

The vortex pinning produced by a random distribution of particles larger than ξ was discussed by van der Beek *et al.*,[33] who predicted a power law with $\alpha = 5/8 = 0.625$ (previous studies made similar predictions with $\alpha = \frac{1}{2}$).[34] For noninteractive vortices (low H) $J_c \approx 0.14 n^{1/2} \gamma [DF(T)]^{3/2} J_0$, where n is the density of the pinning particles, D is their diameter (assuming that they are spherical), $F(T) \approx \ln[1 + D^2/8\xi^2(T)]$, and $J_0 = cH_c/3\sqrt{6}\pi\lambda$ is the depairing current density.[33] For a simple estimate, we can take $F(T) \sim 1$ (a good approximation for D a few times ξ), thus $[DF(T)]^{3/2} \sim (2v)^{1/2}$, where v is the volume of one particle, and $J_c \approx 0.14\gamma(2nv)^{1/2} J_0$. Note that nv is the fraction of the volume occupied by the defects. Using our experimental ξ and λ values, we estimate $J_0(5\text{K}) \approx 500$ M A cm^{-2}, and from Fig. 7(a) $J_c(5\text{K}) \approx 1$ M A cm^{-2}, thus $nv \sim 4 \times 10^{-5}$ not surprisingly indicating that a rather small volume fraction of strong pinning centers is enough to account for the observed $J_c/J_0 \sim 2 \times 10^{-3}$. (For comparison, the $BaZrO_3$ inclusions that are frequently used to increase J_c in $YBa_2Cu_3O_7$ films produce optimum results for volume fractions $\sim$0.05.[35]) These strong-pinning defects could appear spontaneously during the single-crystal growth[36] or, alternatively, this behavior could be associated with phase-separated coexistence of AFM and superconducting and normal states as previously observed in $(BaK)Fe_2As_2$ single crystals.[37]

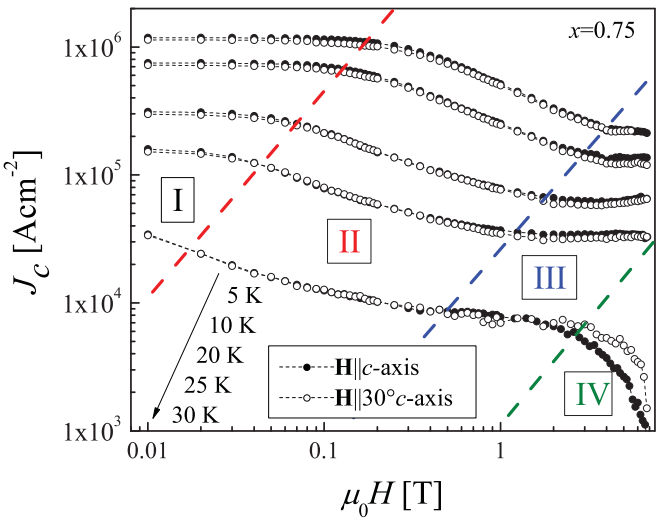

FIG. 8. (Color online) (a) Critical-current density (J_c) as function of magnetic field (H) for $x = 0.75$ with $\mathbf{H} \parallel c$ axis and H rotated 30° from the c axis.

The crossover between the single-vortex limit where J_c is independent of H and the interactive power-law regime should occur at a field $B^* \approx \pi \Phi_0 n(U_p/\varepsilon_0)$, where $U_p \approx \varepsilon_0 DF(T)/4$ is the pinning energy of one nanoparticle and ε_0 is the vortex energy scale. By combining with the J_c result, we obtain $B^* \approx 3\Phi_0(n/\gamma)^{2/3}(J_c/J_0)^{2/3}$, so ideally we could determine n from the crossover between regimes I and II. Unfortunately, our experimental B^* is likely affected by self-field effects, as indicated by the fact that for each temperature $B^*(T) \sim J_c(T)t$, thus, we only have an upper limit for the crossover field, for instance, from $B^*(5\text{ K}) \leqslant 0.2$ T, we obtain $n \leqslant 2 \times 10^{17}$ cm^{-3}.

It should be noted that, according to Koshelev,[38] $J_c(\Theta)$ for nanoparticle pinning does not follow the anisotropic scaling, and in fact depends on both γ and the shape (aspect ratio of main dimensions) of the particles. For instance, for spherical particles (we have no reason to assume otherwise) below B^*, he finds $J_c(\Theta) \propto (\cos^2\Theta + \gamma^{-2}\sin^2\Theta)^{1/4}$, but for $\Theta = 30°$, this factor is $\sim$0.95, too close to 1 to be detectable in our measurements.

According to existing models, regime III can not arise from the same nanoparticles that generate the $\alpha = 5/8$ (or 1/2) regime; instead, above regime II, the models predict another power-law region with $\alpha = 1$, which we do not observe.[33] A natural interpretation is that, as the nanoparticle pinning decreases with increasing H, a new pinning source becomes dominant. The obvious possibility is a much denser distribution of smaller random defects.

C. Regime III

We could try to describe regime III in terms of the collective pinning by random *point* disorder as described by the Larkin-Ovchinnikov (LO) theory,[39] which is consistent with both the low J_c and the anisotropic scaling. However, we find a serious numerical discrepancy regarding the upper boundary of this single-vortex pinning regime. In $x = 0.75$, regime III is visible over a wide range of temperatures, 5 K $< T <$ 25 K, all the way up to our maximum magnetic field $\mu_0 H \sim 6.5$ T, and at 30 K it is still visible over a restricted field range. In the LO scenario, J_c in the single-vortex regime (where J_c is independent of H) is determined by the collective pinning length (Larkin length L_c), and the crossover to the collective pinning of vortex bundles (3D) occurs at a field B_{sb} such that the vortex lattice parameter $a_0 \sim L_c$. According to Blatter *et al.*,[26] in an anisotropic superconductor for $\mathbf{H} \parallel c$, we have $L_c^c = \gamma^{-1}\xi(J_0/J_c)^{1/2}$ and $B_{sb} = \beta_{sb}\frac{J_c}{J_0}H_{c2}$, with $\beta_{sb} \approx 5$. In regime III, $J_c(5\text{ K}) \sim 2.5 \times 10^5$ A cm^{-2} and $J_c(25\text{ K}) \sim 4 \times 10^4$ A cm^{-2}, with $J_0(5\text{ K}) \sim 500$ M A cm^{-2} and $J_0(25\text{ K}) \sim 110$ M A cm^{-2}, while we can estimate $H_{c2}(5\text{ K}) \sim 80$ T and $H_{c2}(25\text{ K}) \sim 33$ T. We thus obtain $B_{sb}(5\text{ K}) \sim 0.2$ T and $B_{sb}(25\text{ K}) \sim 0.06$ T, while our experimental results would imply that $B_{sb} > 6.5$ T at both temperatures, i.e., two orders of magnitude higher than the expectation.

Alternatively, we can again describe this dense distribution of random defects in the van der Beek nanoparticles scenario, thus,

$$B^* \approx 3\Phi_0(n/\gamma)^{2/3}(J_c/J_0)^{2/3} \approx 18\gamma^{-2/3}(\xi/d)^2(J_c/J_0)^{2/3}H_{c2},$$

where d is the average distance between nanoparticles. In this case, the weaker dependence on J_c/J_0 as compared to the LO model allows us to estimate a higher value $B^*(5\text{ K}) \sim (5T)(\xi/d)^2$, but even for a very dense distribution, we can get at most $B^* \sim 1$ T, closer but still below the experimental result (>6.5 T).

To summarize, the regime III in $x = 0.75$ can not be explained by the LO scenario for single-vortex pinning. Considering the numerical uncertainties involved in the analysis, the van der Beek model could be marginally consistent with the observed B^* if we assume a very dense distribution of smaller nanoparticles. It is still possible that this regime arises from a single type of disorder, but we lack of the correct model to describe it. A more interesting alternative is that a mixed pinning landscape is involved. A $J_c(H) \sim constant$ is usually associated with single-vortex pinning, but in more general terms, it is consistent with an interactive vortex regime if the volume of the bundle is independent of H. Although this is not the case for a single type of disorder, we propose that it may occur due to the simultaneous presence of sparse large (strong) nanoparticles and a much denser distribution of smaller particles or pointlike pinning. In this scenario, the sparse pins could produce a caging effect, constraining the volume of the vortex bundle associated with the denser and weaker defects. This points to the importance of improving our understanding of mixed pinning landscapes and hierarchies of pinning scales, and deserves further study. In particular, flux creep studies should provide complementary information.

This scenario is supported by previous studies in pnictide single crystals, which indicate that different kinds of disorder such as phase-separated coexistence of AFM and superconducting and normal states,[37] crystalline defect such as twin domains, impurities, or precipitation, and nanoscopic secondary phases[40] have an important role in the vortex dynamic. Also, a similar scenario has been proposed in YBCO thin films where the vortices sense the pinning potential from correlated defects along the *ab* plane as well as the *intrinsic pinning* from a much larger density of weaker pinning centers. After an initial fall with H, $J_c(\mathbf{H}\|ab)$ stays flat.[41]

D. Regime IV

To investigate regime IV, where $J_c(H)$ decreases to zero, we have analyzed the field dependence of the pinning force $F_P = J_c H$. It has long been known that,[42] if the same pinning mechanism dominates over a certain temperature range, frequently $F_p(H,T)$ can be scaled as $F_P/F_{P,\max} = Ah^m(1-h)^l$, where $F_{p,\max}$ is the maximum $F_p(H)$ at each temperature, A is a constant, m and l are exponents that depend on the pinning mechanism, and $h = H/H_{c2}(T)$. The absence of scaling indicates that different pinning mechanisms occur over the T range investigated. Figure 9 shows the $F_p/F_{p,\max}(h)$ dependence for $x = 0.5$ and 0.75. Following a common procedure for HTS and iron arsenides, we have used $H_{\text{irr}}(T)$ instead of $H_{c2}(T)$ in the definition of h. The $x = 0.5$ [see Figs. 9 and 9(b)] presents a clear change in the pinning mechanism between 8 and 10 K, as evidenced by a shift in the field where the maximum F_p occurs ($h_{\max}$), from ~0.5 to ~0.25 as T is increased from 8 to 10 K. The graphs only include data for $T > 8$ K, the range where we can estimate H_{irr}. In the case of $x = 0.75$, we are constrained to $T \geqslant 30$ K. In this narrow range, we observe $h_{\max} \sim 0.5$. Previous studies in FeAs superconductors have reported $F_p/F_{p,\max}(h)$ with different $h_{\max}$, for example, $h_{\max} \sim 0.33$ and 0.43 in (Ba,K)Fe_2As_2, or $h_{\max} \sim 0.5$ and 0.37 in Co-doped $BaFe_2As_2$,[20,43,44] suggesting that the sample preparation process affects the mechanism that determines the pinning. In our study, we found that differences in doping also affect the vortex dynamics and pinning mechanisms. It is tempting to relate the functional form of $F_p/F_{p,\max}(h)$ to a microscopic pinning mechanism as was done for conventional superconductors, but such analysis is valid for h defined using $H_{c2}(T)$ rather than $H_{\text{irr}}(T)$, so it can not be directly applied here.

E. Comparison with pinning mechanisms in $YBa_2Cu_3O_7$

It is worth comparing the vortex pinning in our FeAs superconductors with those in cuprates, particularly with $YBa_2Cu_3O_7$ (YBCO). The $J_c(H)$ curves at low T for clean YBCO single crystals frequently resemble those of Fig. 7 in several regards, showing a small $J_c \sim constant$ at low H, followed by a decreasing $J_c(H)$ and then another $J_c \sim constant$ region at higher H. In some studies, this regime III was found to extend up to several Tesla (for $T < 20$ K),[45] and repeating the above analysis [for $J_c(5\text{ K}) \sim 0.5$–1 M A cm^{-2}, $J_0(5\text{ K}) \sim$ 300 M A cm^{-2}, and $H_{c2}(5\text{ K}) \sim 120$ T], we find $B_{sb}(5\text{ K}) \sim$ 1–2 T, again lower than the experimentally observed upper bound of the regime III, although the discrepancy is much smaller than in the FeAs crystals of this study. The B^* estimate for a very dense distribution of nanoparticles, on the other hand, could explain the regime III in YBCO. At intermediate temperatures, many YBCO crystals show a SPM, attributed to various crystallographic defects such as oxygen deficiency or antiphase boundaries, but it has been shown that the SPM can be removed by annealing,[46] leaving a much reduced $J_c \sim constant$ component. A similar relation between the SPM and the high field $J_c \sim constant$ may occur in the pnictides.

The comparison with YBCO films is more difficult. An important difference is that J_c in YBCO films is much higher than either in YBCO or FeAs single crystals, reaching a significant fraction of the depairing limit. In general, films show an initial $J_c \sim constant$ regime followed by a decreasing $J_c(H)$, but no regime III at high fields. This may be simply because the "low-field" component of the pinning is much stronger and remains significant up to fields approaching H_{irr}. Depending on the deposition method, some standard YBCO films show a power-law regime with similar α values than our 122 crystals, even though nanoparticles are not present (at least in significant densities). In those cases, the $\alpha \sim 0.5$–0.6 is associated with random defects and/or combination of those with c-axis correlated disorder (dislocations, twin boundaries).

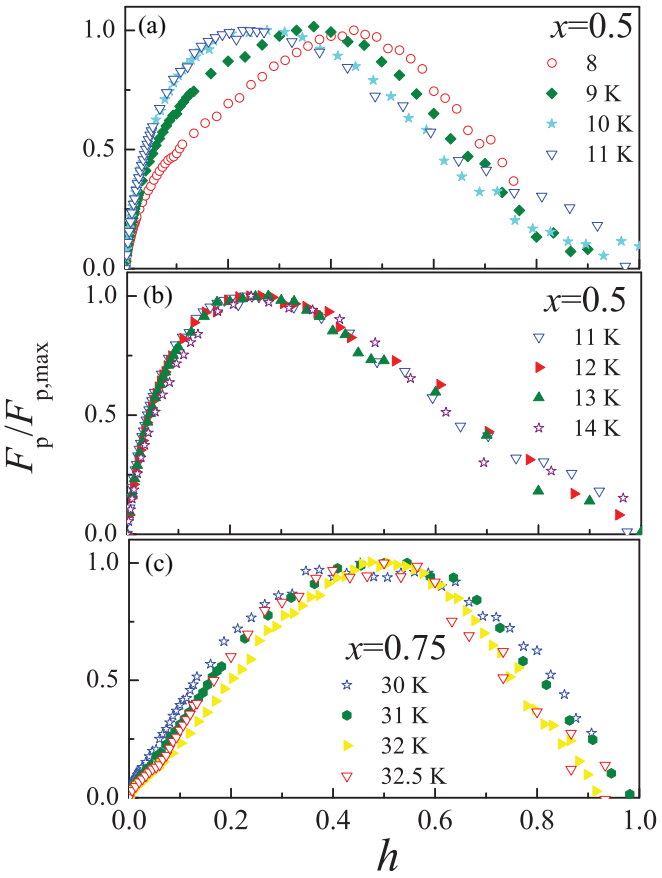

FIG. 9. (Color online) Normalized pinning force (F_p) versus normalized magnetic field [$h = H/H_{irr}(T)$] at different temperatures. (a) and (b) $x = 0.5$. (c) $x = 0.75$.

On the other hand, YBCO films in which a large density of nanoparticles is the dominant pinning source show no power-law dependence.[47,48]

V. CONCLUSIONS

In conclusion, we have investigated the effect of Na doping on the superconducting properties of $Ca_{1-x}Na_xFe_2As_2$ single crystals. The maximum T_c in this material corresponds to a chemical doping different from $(Ba,K)Fe_2As_2$ and $(Sr,K)Fe_2As_2$. Scaling of the upper critical field H_{c2} versus T indicates that our samples show a single-band-like behavior close to T_c with a $\gamma = 1.85 \pm 0.05$, independently of the chemical doping and T_c value. A narrow vortex liquid phase was detected in the sample with highest T_c ($x = 0.75$), in agreement with the expectations from the superconducting properties T_c, H_{c2}, and G_i. The field and angular dependence of the critical-current density in both the underdoped and optimally doped single crystals indicates that pinning arises from a combination of several mechanisms. At low fields, pinning by random nanoparticles dominates. At higher fields, a small and field independent J_c in the optimally doped crystal may originate in the simultaneous presence of sparse large nanoparticles and a much denser distribution of smaller particles, with the sparse pins producing a caging effect that constrains the volume of the vortex bundle associated with the denser and weaker defects. No evidence of directional pinning by correlated disorder is observed. More studies are necessary in order to understand the influence of the different crystalline defects on the vortex pinning and dynamics of these materials.

ACKNOWLEDGMENTS

We thank Cristian Batista for useful discussions and a careful reading of the manuscript. Research at LANL was supported by the US Department of Energy, Office of Basic Energy Sciences, Division of Materials Sciences and Engineering (XRD, EDX, Rutherford backscattering, magnetometry, data analysis, manuscript preparation), and by NSF-DMR-0654118, DOE, and the State of Florida (transport measurements at The National High Magnetic Field Laboratory - Pulsed Field Facility at LANL). Work by G.F.C. and W.Y. (fabrication of samples) was supported by the NSFC under Grants No. 10974254 and No. 11074304, and by the National Basic Research Program of China under Grants No. 2010CB923000 and No. 2011CBA00100. N. H. is member of CONICET (Argentina).

[1] Y. Kamihara, T. Watanabe, M. Hirano, and H. J. Hosono, J. Am. Chem. Soc. **130**, 3296 (2008).
[2] J. Paglione and R. L. Greene, Nat. Phys. **6**, 645 (2010).
[3] G. Wu, H. Chen, T. Wu, X. L. Xie, Y. J. Yan, R. H. Liu, X. F. Wang, J. J. Ying, and X. H. Chen, J. Phys.: Condens. Matter **20**, 422201 (2008).
[4] P. M. Shirage, K. Miyazawa, H. Kito, H. Eisaki, and A. Iyo, Appl. Phys. Express **1**, 081702 (2008).
[5] M. Gooch, B. Lv, K. Sasmal, J. H. Tapp, Z. J. Tang, A. M. Guloy, B. Lorenz, and C. W. Chu, J. Phys. C **470**, 276 (2010).
[6] H. L. Shi, H. X. Yang, H. F. Tian, J. B. Lu, Z. W. Wang, Y. B. Qin, Y. J. Song, and J. Q. Li, J. Phys.: Condens. Matter **22**, 125702 (2010).
[7] M. S. Torikachvili, S. L. Bud'ko, N. Ni, and P. C. Canfield, Phys. Rev. Lett. **101**, 057006 (2008).
[8] E. Colombier, S. L. Ni Bud'ko, and P. C. Canfield, Phys. Rev. B **79**, 224518 (2009).
[9] K. Zhao, Q. Q. Liu, X. C. Wang, Z. Deng, Y. X. lv, J. L. Zhu, F. Y. Li, and C. Q. Jin, J. Phys.: Condens. Matter **22**, 222203 (2010).
[10] M. Rotter, M. Tegel, and D. Johrendt, Phys. Rev. Lett. **101**, 107006 (2008).
[11] G. F. Chen, Z. Li, G. Li, W. Z. Hu, J. Dong, X. D. Zhang, P. Zheng, N. L. Wang, and J. L. Luo, Chin. Phys. Lett. **25**, 3403 (2008).
[12] A. V. Chubukov, D. V. Efremov, and I. Eremin, Phys. Rev. B **78**, 134512 (2008).
[13] H. Shishido *et al.*, Phys. Rev. Lett. **104**, 057008 (2010).
[14] S. A. Baily, Y. Kohama, H. Hiramatsu, B. Maiorov, F. F. Balakirev, M. Hirano, and H. Hosono, Phys. Rev. Lett. **102**, 117004 (2009).

[15]F. Hunte, J. Jaroszynski, A. Gurevich, D. C. Larbalestier, R. Jin, A. S. Sefat, M. A. McGuire, B. C. Sales, D. K. Christen, and D. Mandrus, Nature (London) **453**, 903 (2008).
[16]H. Q. Yuan, J. Singleton, F. F. Balakirev, S. A. Baily, G. F. Chen, J. L. Luo, and N. L. Wang, Nature (London) **457**, 33 (2009).
[17]M. M. Altarawneh, K. Collar, C. H. Mielke, N. Ni, S. L. Bud'ko, and P. C. Canfield, Phys. Rev. B **78**, 220505 (2008).
[18]Z.-S. Wang, Hui-qian Luo, C. Ren, and Hai-hu Wen, Phys. Rev. B **78**, 140501 (2008).
[19]N. Ni, L. Budko, A. Kreyssig, S. Nandi, D. E. Rustan, A. I. Goldman, S. Gupta, J. D. Corbett, A. Kracher, and P. C. Canfield, Phys. Rev. B **78**, 14507 (2008).
[20]H. Yang, Hui-qian Luo, Z. Wang, and Hai-Hu Wen, Appl. Phys. Lett. **93,** 142506 (2008).
[21]H.-J. Kim, Y. Liu, Y. S. Oh, S. Khim, I. Kim, G. R. Stewart, and K. H. Kim, Phys. Rev. B **79**, 014514 (2009).
[22]A. Yamamoto, J. Jaroszynski, C. Tarantini, L. Balicas, J. Jiang, A. Gurevich, D. C. Larbalestier, R. Jin, A. S. Sefat, M. A. McGuire, B. C. Sales, D. K. Christen, and D. Mandrus, Appl. Phys. Lett. **94**, 062511 (2009).
[23]B. Maiorov, T. Katase, S. A. Baily, H. Hiramatsu, T. G. Holesinger, H. Hosono, and L. Civale, Supercond. Sci. Technol. **24**, 055007 (2011).
[24]K. Prokeš, S. Mat'aš, L. Harnagea, S. Singh, S. Wurmehl, D. N. Argyriou, and B. Büchner, Phys. Rev. B **83**, 104414 (2011).
[25]R. Prozorov, M. A. Tanatar, B. Shen, P. Cheng, H.-H. Wen, S. L. Bud'ko, and P. C. Canfield, Phys. Rev. B **82**, 180513 (2010).
[26]G. Blatter, M. V. Feigel'man, V. B. Geshkenbein, A. I. Larkin, and V. M. Vinokur, Rev. Mod. Phys. **66**, 1125 (1994).
[27]M. Tinkham, *Introduction to Superconductivity,* 2nd ed. (Dover, New York, 2004).
[28]B. Maiorov *et al.*, Phys. Rev. B **61**, 12427 (2000).
[29]L. Civale *et al.*, Appl. Phys. Lett. **84**, 2121 (2004).
[30]R. Prozorov, M. A. Tanatar, N. Ni, A. Kreyssig, S. Nandi, S. L. Bud'ko, A. I. Goldman, and P. C. Canfield, Phys. Rev. B **80**, 174517 (2009).
[31]H. Yang, H. Luo, Z. Wang, and H.-H. Wen, Appl. Phys. Lett. **93**, 142506 (2008).
[32]R. Prozorov, N. Ni, M. A. Tanatar, V. G. Kogan, R. T. Gordon, C. Martin, E. C. Blombeerg, P. Prommapan, J. Q. Yan, S. L. Bud'ko, and P. C. Canfield, Phys. Rev. B **78**, 224506 (2008).
[33]C. J. van der Beek, M. Konczykowski, A. Abal'oshev, I. Abal'osheva, P. Gierlowski, S. J. Lewandowski, M. V. Indenbom, and S. Barbanera, Phys. Rev. B **66**, 024523 (2002).
[34]V. M. Vinokur, B. Khaykovich, E. Zeldov, M. Konczykowski, R. A. Doyle, and P. H. Kes, Phys. C (Amsterdam) **295**, 209 (1998).
[35]J. L. Macmanus-Driscoll, S. R. Foltyn, Q. X. Jia, H. Wang, A. Serquis, L. Civale, B. Maiorov, M. E. Hawley, M. P. Maley, and D. E. Peterson, Nat. Mater. **3**, 439 (2004).
[36]C. J. van der Beek *et al.*, Phys. Rev. B **81**, 174517 (2010).
[37]J. T. Park *et al.*, Phys. Rev. Lett. **102**, 117006 (2009)
[38]A. E. Koshelev (private communication).
[39]A. I. Larkin and Yu. N. Ovchinnikov, J. Low Temp. Phys. **34**, 409 (1979).
[40]Yi Yin *et al.*, Phys. Rev. Lett. **102**, 097002 (2009).
[41]L. Civale, B. Maiorov, J. L. MacManus-Driscoll, H. Wang, T. G. Holesinger, S. R. Foltyn, A. Serquis, and P. N. Arendt, IEEE Trans. Appl. Supercond. **15**, 2808 (2005).
[42]D. Dew-Hughes, Philos. Mag. **30**, 293 (1974).
[43]D. L. Sun, Y. Liu, and C. T. Lin, Phys. Rev. B **80**, 144515 (2009).
[44]A. Yamamoto, J. Jaroszynski, C. Tarantini, L. Balicas, J. Jiang, A. Gurevich, D. C. Larbalestier, R. Jin, A. S. Sefat, M. A. McGuire, B. C. Sales, D. K. Christen, and D. Mandrus, Appl. Phys. Lett. **94**, 062511 (2009).
[45]L. Civale, L. Krusin-Elbaum, J. Thompson, and F. Holtzberg, Phys. Rev. B. **50**, 7188 (1994).
[46]J. Shibata, A. Oka, T. Izumi, Y. Shiohara, T. Hirayama, and Y. Ikuhara, J. Mater. Res. **16**, 1935 (2001).
[47]V. F. Solovyov, H. J. Wiesmann, L. Wu, Q. Li, L. D. Cooley, M. Suenaga, B. Maiorov, and L. Civale, Supercond. Sci. Technol. **20**, L20 (2007).
[48]B. Maiorov, S. A. Baily, H. Zhou, O. Ugurlu, J. A. Kennison, P. C. Dowden, T. G. Holesinger, S. R. Foltyn, and L. Civale, Nat. Mater. **8**, 398 (2009).